Groeger, S; Bison, G; Knowles, PE; Wynands, R; Weis, A

Laser-pumped cesium magnetometers for high-resolution medical and fundamental research

SENSORS AND ACTUATORS A: PHYSICAL, 129 (2006) 1-5

published May 2006

Laser-pumped cesium magnetometers for high resolution medical and fundamental research

S. Groeger[a], G. Bison[a], P. E. Knowles[a], R. Wynands[b], A. Weis[a]

[a] University of Fribourg, Physics Department, 1700 Fribourg, Switzerland

[b] PTB 4.41, 38116 Braunschweig, Germany

Abstract

Laser-pumped cesium magnetometers allow highly sensitive magnetometry at room temperature. We report on applications of that technique in biomagnetic diagnostics and in a neutron electric dipole moment (nEDM) experiment. In the biomagnetic application the magnetic field from the beating human heart is detected using a gradiometer which reaches an intrinsic sensitivity of 80 fT/Hz$^{1/2}$. The device can record time-resolved magnetic field maps above the human body surface with a spatial resolution of 4 cm and its performance is comparable to commercial devices based on the SQUID technique. In the nEDM experiment laser-pumped cesium magnetometers are used to measure and stabilize a DC magnetic field at a level of 10^{-7}. Those devices reach an intrinsic sensitivity of about 14 fT/Hz$^{1/2}$ with a measurement bandwidth of 1 kHz. The general principle of operation and specific results are presented.

Keywords: optical magnetometry, spin physics, cardiomagnetometry, magnetocardiogram, electric dipole moment

Introduction

In many areas of fundamental and applied science the sensitive detection of weak magnetic fields and small field fluctuations is of great importance. Experiments looking for small violations of discrete symmetries in atoms and particles (such as the neutron) require precise control of the magnetic field. In past experiments looking for an electric dipole moment (EDM) of the neutron magnetic fields were measured by optically pumped alkali magnetometers, which monitored the field at several positions outside the neutron experimental volume [1], or by optically pumped ^{199}Hg, which acted as a comagnetometer in the volume occupied by the neutrons [2]. The precession frequency of ^{199}Hg in a 1 μT field is about 8 Hz, and the time resolution for that magnetometer type is very low. In contrast to this, optically pumped cesium magnetometers offer the possibility for fast real-time field measurements with more than 100 times larger bandwidth due to the larger gyromagnetic ratio and variable spatial resolution. That property is very important in our second area of interest, the measurement of magnetic fields produced by biological organisms, which contain valuable information on the underlying physiological processes and associated pathologies [3]. Currently superconducting quantum interference devices (SQUID) cooled far below room temperature were required to measure those weak biomagnetic signals. The requirements for a useful magnetic field sensor for biomagnetic detection are, besides an ultra-high sensitivity, a time resolution in the millisecond range and a spatial resolution on the cm-scale, conditions which both can be met by optically pumped cesium magnetometers.

Optically pumped magnetometers

The principle of optically pumped magnetometers (OPM) using alkali vapors was developed in the second half of the last century using discharge lamps as light sources [4]. Since then a steady development in electronics and in semiconductor laser technology has allowed the development of devices with sensitivities of a few fT/Hz$^{1/2}$ [5] or less [6]. Here we introduce the OPM technique as employed by our group.

The scheme of an OPM is shown in Fig. 1. A circularly polarized light beam (from a tunable extended-cavity diode laser) traverses a vapor of cesium atoms. The light frequency is tuned to the $\left(6^2\mathrm{S}_{1/2}\right)F=4 \rightarrow \left(6^2\mathrm{P}_{1/2}\right)F=3$ hyperfine transition of the D_1 line at 894 nm, and the laser frequency is locked by a dichroic atomic vapor laser lock (DAVLL) [7], which provides a continuous stable operation over weeks. Due to optical pumping [8] the

equilibrium populations of the Zeeman substates in the sample are changed and a macroscopic net magnetization is induced along the light propagation direction. In an external magnetic field B_0, the magnetization precesses around the field direction with the Larmor frequency $\omega_L = 2\pi\gamma B_0$, where γ=3.5 Hz/nT is the gyromagnetic ratio of Cs. The measurement of the magnetic field is thus transferred to a frequency measurement. In the geometry used here, the so-called M_x configuration, B_0 subtends an angle of 45° with the light propagation direction. The precession is resonantly driven by a transverse radiofrequency (r.f.) field $B_1(t)$ oscillating at the frequency ω_{rf}, which leads to a periodically changing projection of the magnetization on the light direction at the frequency ω_{rf}. This results in a modulation of the optical absorption coefficient and thus of the light power transmitted through the cesium sample. That modulation can be monitored by detecting either its in-phase component, its quadrature component, or its phase with respect to the oscillating r.f. field. All three signals show a resonant behavior when ω_{rf} is scanned across ω_L; in particular the phase on resonance is –90°.

The magnetometer is operated by actively stabilizing ω_{rf}, generated by a voltage controlled oscillator (VCO), to the Larmor frequency by an electronic feedback loop, and the magnetometer signal is obtained by measuring the radiofrequency ω_{rf} in the locked mode. Both the in-phase and the phase signals have a dispersive dependence on the detuning which provide an error signal for the servo loop in order to lock the phase to –90°. The magnetometer is then said to be operated in the phase-stabilized mode. The magnetic field range of the magnetometer is limited by the frequency range of the VCO, whereas the response bandwidth to magnetic field changes depends on the loop filters. Note that in principle the maximum bandwidth of an optically pumped magnetometer is given by the Larmor frequency of the atoms.

The resolution of a magnetic field measurement depends on the noise equivalent magnetic field (NEM) which is the magnetic field change δB that induces a detector signal equivalent to the signal noise

$$\delta B = \delta B_{\text{int}} + \delta B_{\text{ext}}, \qquad (1)$$

where δB_{int} is the noise inherent to the magnetometer and δB_{ext} are magnetic field fluctuations. The NEM δB_{int} can be determined directly only from the noise of a magnetic field measurement in a perfectly stable field ($\delta B_{\text{ext}} = 0$). In that case the Fourier spectrum of the OPM signal would show a single peak at the Larmor frequency (carrier) superposed on a noise background corresponding to the magnetometer noise. Magnetic field fluctuations, as well as, e.g., laser power fluctuations or electronic noise, will appear as sidebands of the carrier in the Fourier spectrum. Equation (1) can thus be written as

$$\delta B = \frac{1}{\gamma}\frac{\Delta\nu}{S/N}, \qquad (2)$$

where $\Delta\nu$ is the half linewidth of the resonance and S/N the signal-to-noise ratio of the modulation signal at the Larmor frequency. The noise level $N\left(=\sqrt{N_{\mathrm{SN}}^2 + N_{\mathrm{OPM}}^2 + N_{\mathrm{ext}}^2}\right)$, measured in a bandwidth f_{bw}, consists of the shot noise N_{SN} originating from the current noise $\Delta I\left(=\sqrt{2eI_{\mathrm{pc}}\, f_{\mathrm{bw}}}\right)$ of the photodiode current I_{pc}, the noise inherent to the magnetometer proper, N_{OPM}, and external field fluctuations which can be parametrized as N_{ext}. In Fig. 2 a typical FFT spectrum of an OPM inside a three-layer magnetic shield is shown. The peak at the Larmor frequency is superposed on a broad pedestal that stems from external magnetic field fluctuations. The sidebands at 50 Hz appear due to an incomplete shielding of the power-line field. The white noise floor in the far wings of the spectrum corresponds to $N_{\mathrm{int}}\left(=\sqrt{N_{\mathrm{SN}}^2 + N_{\mathrm{OPM}}^2}\right)$ at the carrier frequency and allows us to infer the inherent magnetometer NEM δB_{int}.

Magnetometers for a neutron electric dipole moment experiment

It is well known that the discrete symmetries P (parity conservation) and T (time reversal invariance) forbid that elementary particles with nonzero spin have a permanent electric dipole moment (EDM). The experimental search for a finite EDM is thus a search for P- and T-violating effects in elementary particles or composite systems, such as atoms or molecules [9]. We participate in the planning of a new neutron EDM experiment at the ultra-cold neutron source under construction at the Paul Scherrer Institute (PSI), Switzerland [10]. For symmetry reasons an EDM has to be parallel or antiparallel to the total angular momentum of the system under investigation so that a change of the EDM's orientation by an external electric field will affect the spin coherence and thereby the sample magnetization. Practically all ongoing EDM experiments make use of that effect by looking for a change of a magnetic resonance frequency induced by a static electric field applied parallel/antiparallel to a magnetic field. The signature of an EDM will be a tiny change of the precession frequencies in the two geometries. A signal that could mimic an EDM can arise when the magnetic field seen by the neutrons changes during the neutron spin precession time (typically on the order of hundred seconds). In order to control field drift effects, Cs-OPMs will be used to measure and correct such field fluctuations at the level of a few fT, which places very strict requirements on the OPM sensitivity.

The magnetometers used for the neutron EDM experiment consist of three parts (Fig. 1): a) a sensor head containing no metallic parts except the r.f. coils, b) the feedback electronics, and c) a base station mounted in a portable 19" rack drawer, which contains the frequency stabilized laser and all optics. Note that only one base station is needed in the experiment, since a single diode laser can produce sufficient light power to drive all sensors in the experiment. The 242 mm long sensor head is designed to fit into a tube of 104 mm diameter, coaxial with a static 2 μT field. Its main component is an internally paraffin-coated 7 cm diameter glass cell containing a droplet of cesium. The pumping light is guided from the base station to the sensor head via a 10 m long multimode fiber (core diameter: 800 μm). The modulated light transmitted by the cesium vapor is fed back to a photodiode in the electronics unit by a similar fiber. Multimode fibers were used instead of single mode fibers because of the easier light coupling – especially for guiding the light back from the sensor head. Multimode fibers in principle change the polarization of the light depending on the applied stress. We found that a few loops in the fiber with a diameter of about 5 cm produces unpolarized light at the fiber output. Thus the power transmitted by the linear polarizer is independent of the fiber position. The photodiode signal is analyzed by a dual-channel lock-in amplifier, referenced to the r.f. coil driving frequency produced by a voltage controlled oscillator (VCO). Either the phase or the dispersive in-phase output of the lock-in amplifier can be used in a feedback loop to lock the driving frequency to the Larmor frequency by stabilizing the phase shift to –90°. The temporal response of the phase-stabilized magnetometer to field changes, i.e., its bandwidth, can be adjusted up to 1 kHz by changing the loop filters. The intrinsic sensitivity is $\delta B_{\mathrm{int}} = 14\ \mathrm{fT/Hz^{1/2}}$. Figure 3 plots the Allan standard deviation [11] of magnetic field fluctuations recorded during several hours inside a three-layer Mumetal shield. One can see that the measured stability of the 2 μT field lies one to two orders of magnitude above the intrinsic sensitivity. The field fluctuations show a white noise behavior for short integration times and are due to slow field drifts for long integration times. The plateau in the range of 2 to 100 s is caused by current fluctuations at the level of 10^{-7} in the solenoid producing the magnetic field. Details of the characterization and performance of the device are given in [12].

Magnetocardiography

Our biomagnetic research is focused on the detection of human cardiomagnetic fields. In the M_x configuration, the intrinsically scalar OPM is mainly sensitive to the cardiomagnetic field component along an externally applied bias field, and thus operates as an effective vector magnetometer (Fig. 4a). The current intrinsic

sensitivity of the magnetometer is 80 fT/Hz$^{1/2}$ with a cylindrical vapor cell of only 6 cm^3. The measurement bandwidth is 100 Hz, which is sufficient to resolve all relevant magnetic features of the magnetocardiogram (MCG). Details of the device are given in [13].

Time-varying stray fields, in particular at the power-line frequency, which are typically many orders of magnitude larger than the strongest peaks of the heart signal (which itself has a maximum value of about 100 pT), can be effectively suppressed by a gradiometric arrangement of two (or more) sensors [14]. So far we have used one sensor near the chest (OPM1) and a second sensor (OPM2) 7 cm away as a reference for stray fields, which are then compensated by a servo loop (Fig. 4a). The OPM1 sensor detects both the heart and the stray signals, while OPM2 records stray fields only. In this way a difference measurement allows us to extract the signal of interest, provided that the stray field homogeneity is. In our first experiments, ambient magnetic field fluctuations were further suppressed by operating the sensors inside a room weakly shielded by a single layer of Mumetal.

Even the unfiltered output data of the gradiometer (Fig. 4b) presents the major features of the human magnetocardiogram. After state-of-the-art filtering based on the noise extraction in state space [15] finer features can be resolved (Fig. 4c). Figure 5 shows a map of the R peak amplitude (the most prominent feature in the MCG), measured at 36 points across the chest of one of the authors [16]. Such maps are a useful tool for biomagnetic studies and medical diagnostics [17]. By averaging traces like those in Fig. 4b it is possible to produce a series of such maps covering the whole cardiac cycle, which then can be combined into a movie of the spatial magnetic field distributions as a function of time [18]. In a mini-trial with two volunteers we have compared the maps and movies of the cardiomagnetic field generated both by our OPM and by a conventional multichannel SQUID system in the group of R. Fenici at the Catholic University of Rome. It was found that both methods yield basically identical results [19].

Conclusion

The possibilities offered by laser light sources have opened up new areas of research and application for optical magnetometry. Not only can these magnetometers be used in fundamental research like the hunt for symmetry-violating permanent electric dipole moments in elementary particles, but they also have a practical advantage, for

instance in the form of laser cardiomagnetometers that can make the benefits of cardiomagnetometry more commonly available.

Acknowledgments

The work described here was supported by Deutsche Forschungsgemeinschaft, Schweizerischer Nationalfonds, INTAS, and Paul-Scherrer-Institute.

Biography

Antoine Weis got his Ph.D. in physics in 1984 at ETH Zürich. He has been full professor at the Physics Department of the University of Fribourg (Switzerland) since 1999 and leader of the Fribourg Atomic Physics group (FRAP). His research topics cover the spectroscopy of atomic defects in quantum crystals and the use of spin coherent samples for the investigation of forbidden and strongly suppressed processes in atoms. Stephan Groeger has been a Ph.D. student in the FRAP group since 2002, whose research is focused on the development of magnetometers for the neutron EDM experiment. Georg Bison got his Ph.D. degree in physics in 2004 for his work on the cardiomagnetometer and is continuing his work as a post-doc in the FRAP group. Paul Knowles got his Ph.D. in physics in 1996 at University of Victoria (Canada) and is working as maître-assistant in the FRAP group. Robert Wynands got his Ph.D. in physics in 1993. He worked on the projects described here as a guest professor in Fribourg and is now working at Physikalisch-Technische Bundesanstalt (PTB) in Braunschweig (Germany) on the development of primary atomic clocks based on cesium.

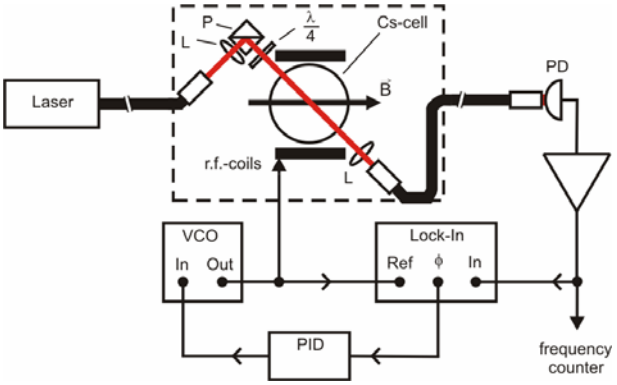

Fig. 1: Schematic setup of the phase-stabilized magnetometer. The dashed box indicates the sensor. L: lens, P: polarizing beamsplitter, λ/4: quarter-wave plate, PD: photodiode, VCO: voltage-controlled oscillator, PID: feedback amplifier. The stabilization system for the laser frequency is not shown.

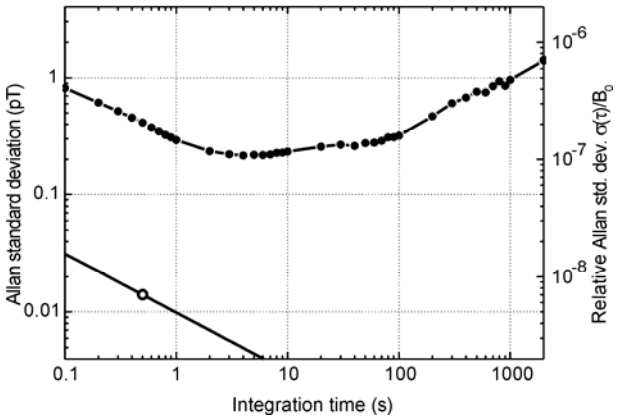

Fig. 3: Upper curve: Allan standard deviation of the magnetic flux density inside the magnetic shield. Lower curve: Magnetometer inherent NEM δB_{int} measured in a 1 Hz bandwidth (circle). The straight line is an extrapolation to other integration times assuming a white noise behavior.

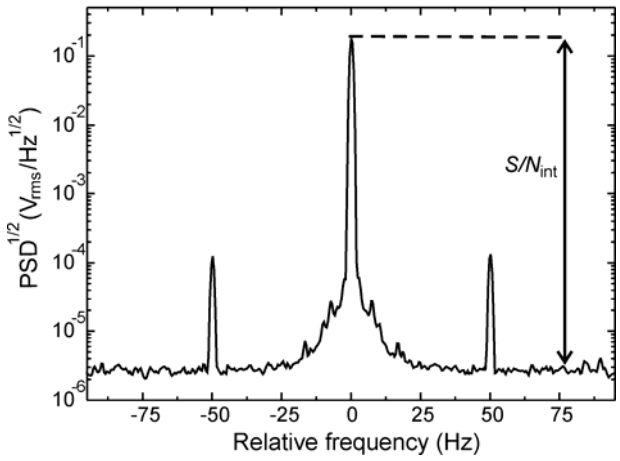

Fig. 2: Square root of the power spectral density (PSD) of the magnetometer output frequency relative to the Larmor frequency of ν_L=7032 Hz (averaged 20 times). The spectrum was measured with a 1 Hz resolution bandwidth. The signal-to-noise ratio S/N_{int} is approximately 66000. The sidebands are due to imperfectly shielded magnetic field components oscillating at the 50-Hz power-line frequency.

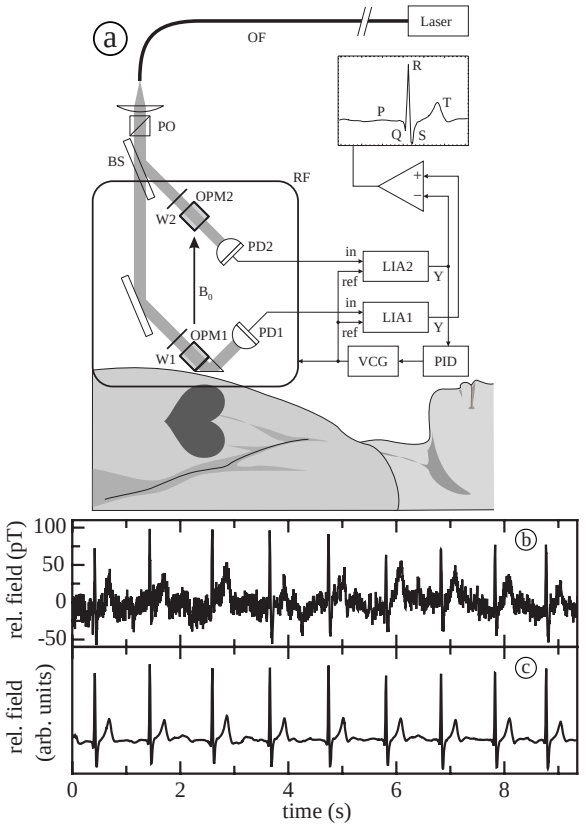

Fig. 4: (a) Experimental setup for MCG recordings (OF: optical fiber, PO: polarizer, BS: polarization maintaining beam splitter, W: quarter-wave plate, PD: photodiode, RF: coil for the r.f. field, VCG: voltage-controlled oscillator, LIA: lock-in amplifier, PID: servo electronics). The inset shows the typical shape and nomenclature of the human magnetocardiogram. (b) Example of the output data of the gradiometer. (c) The same data filtered using state-of-the-art signal recovery techniques based on the noise extraction in state space [15].

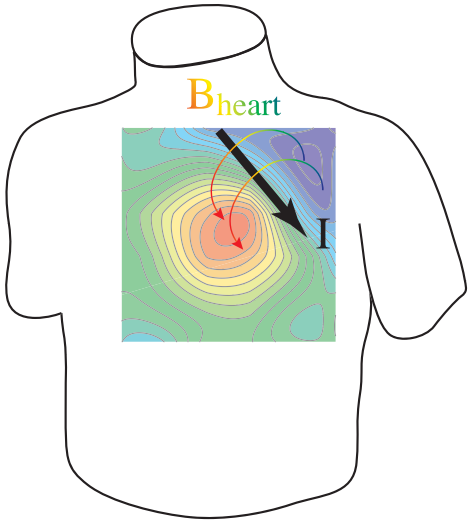

Fig. 5: Map of the R peak of the cardiomagnetic field of one of the authors, with an overlay indicating qualitatively the orientation of the corresponding physiological current and magnetic field lines at the time of the R peak.

Fig. 1: Schematic setup of the phase-stabilized magnetometer. The dashed box indicates the sensor. L: lens, P: polarizing beamsplitter, λ/4: quarter-wave plate, PD: photodiode, VCO: voltage-controlled oscillator, PID: feedback amplifier. The stabilization system for the laser frequency is not shown.

Fig. 2: Square root of the power spectral density (PSD) of the magnetometer output frequency relative to the Larmor frequency of ν_L=7032 Hz (averaged 20 times). The spectrum was measured with a 1 Hz resolution bandwidth. The signal-to-noise ratio S/N_{int} is approximately 66000. The sidebands are due to imperfectly shielded magnetic field components oscillating at the 50-Hz power-line frequency.

Fig. 3: Upper curve: Allan standard deviation of the magnetic flux density inside the magnetic shield. Lower curve: Magnetometer inherent NEM δB_{int} measured in a 1 Hz bandwidth (circle). The straight line is an extrapolation to other integration times assuming a white noise behavior.

Fig. 4: (a) Experimental setup for MCG recordings (OF: optical fiber, PO: polarizer, BS: polarization maintaining beam splitter, W: quarter-wave plate, PD: photodiode, RF: coil for the r.f. field, VCG: voltage-controlled oscillator, LIA: lock-in amplifier, PID: servo electronics). The inset shows the typical shape and nomenclature of the human magnetocardiogram. (b) Example of the output data of the gradiometer. (c) The same data filtered using state-of-the-art signal recovery techniques based on the noise extraction in state space [15].

Fig. 5: Map of the R peak of the cardiomagnetic field of one of the authors, with an overlay indicating qualitatively the orientation of the corresponding physiological current and magnetic field lines at the time of the R peak.

References

1 I. S. Altarev et al., Search for the neutron electric dipole moment, Phys. Atom. Nucl. 59 (1996) 1152 1170

2 K. Green et al., Performance of an atomic mercury magnetometer in the neutron EDM experiment, Nucl. Instr. Meth. A 404 (1998) 381 393

3 W. Andrä and H. Nowak (eds.), *Magnetism in Medicine*, Wiley-VCH, Berlin, 1998.

4 A. L. Bloom, Principles of operation of the Rubidium vapor magnetometer, Appl. Opt. 1 (1962) 61 68.

5 E. B. Aleksandrov et al.,Laser pumping in the scheme of an Mx-magnetometer, Opt. Spectrosc. 78 (1995) 325 332.

6 J. Allred, R. Lyman, T. Kornack, and M. Romalis, High-sensitivity atomic magnetometer unaffected by spin-exchange relaxation, Phys. Rev. Lett. 89 (2002) 130801.

7 V. V. Yashchuk, D. Budker, and J. R. Davis, Laser frequency stabilization using linear magneto-optics, Rev. Sci. Instrum. 71 (2000) 341 346.

8 J. Brossel and A. Kastler, La detection de la resonance magnetique des niveaux excites – l'effect de depolarization des radiations de resonance optique et de fluorescence, Cr. Hebd. Acad. Sci. 229 (1949) 1213 1215.

9 I. B. Khriplovich and S. K. Lamoreaux, *CP violation without strangeness*, Springer Verlag, Berlin, 1997.

10 See http://ucn.web.psi.ch/

11 J. A. Barnes et al., Characterization of frequency stability, IEEE Trans. Instrum. Meas. 20 (1971) 105 120.

12 S. Groeger, J.-L. Schenker, R. Wynands, and A. Weis, A high-sensitive laser-pumped M_x-magnetometer, arXiv:physics/0406105.

13 G. Bison, R. Wynands, and A. Weis, Optimization and performance of an optical cardio-magnetometer, J. Opt. Soc. Am. B 22 (2005) 77 87.

14 C. Affolderbach, M. Stähler, S. Knappe, and R. Wynands, An all-optical, high-sensitivity magnetic gradiometer, Appl. Phys. B 75 (2002) 605 612.

15 K. Sternickel, A. Effern, K. Lehnertz, Th. Schreiber, and P. David, Nonlinear noise reduction using reference data, Phys. Rev. E 63 (2001) 036209-1-4.

16 G. Bison, R. Wynands, and A. Weis, A laser-pumped magnetometer for the mapping of human cardio-magnetic fields, Appl. Phys. B 76 (2003) 325 328.

17 I. Tavarozzi, S. Comani, C. Del Gratta, S. Di Luzio, G. L. Romani, S. Gallina et al., Magnetoardiography: current status and perspectives. Part II: Clinical applications, Ital. Heart J. 3 (2002) 151 165.

18 G. Bison, R. Wynands, A. Weis, Dynamical mapping of the human cardiomagnetic field with a room-temperature, laser-optical sensor, Optics Express 11 (2003) 904 909.

19 R. Fenici, G. Bison, R. Wynands, D. Brisinda, A. M. Meloni, and A. Weis, Comparison of magnetocardiographic mapping with SQUID-based and laser-pumped magnetometers in normal subjects, NFSI 2003: 4th International Conference on Noninvasive Functional Source Imaging, Chieti, Italy, Sept. 10 13, 2003

Stephan Groeger

Physics Department
University of Fribourg
Chemin de Musée 3
1700 Fribourg
Switzerland

TEL: +41 26 300 9035
FAX: +41 26 300 9631

stephan.groeger@unifr.ch

(The manuscript consists of 12 pages)